Measurement of the Longitudinal Energy Distribution of Electrons in Low Energy Beams using Electrostatic Elements

LJ Devlin,[1,2] LB Jones,[1,3] TCQ Noakes,[1,3] CP Welsch,[1,2] and BL Militsyn[1,3]
[1)]*The Cockcroft Institute, Sci-Tech Daresbury, Warrington, UK*
[2)]*The University of Liverpool, Liverpool, UK*
[3)]*ASTeC, STFC, Sci-Tech Daresbury, Warrington, UK*

(Dated: 25 August 2018)

The Transverse Energy Spread Spectrometer (TESS) was designed primarily to study the mean transverse energy spread of electrons emitted from photocathode electron sources at both room and liquid nitrogen temperatures as a function of quantum efficiency through analysis of the photoemission footprint. By reconfiguring the potentials applied to different detector elements, TESS can also be used to measure the mean longitudinal energy spread of photoemitted electrons. Initial plans were to use electrostatic wire meshes as a retarding element which prevents the detection of electrons with insufficient energy to overcome a variable potential barrier. However, this method has proved impractical and a new method has been proposed in which the photocathode bias potential is swept (effectively from a state of no electron emission to full emission) and the emitted photocurrent is then detected by a photoemitted charge collector. In this article, we present the TESS set-up and analyse this new method to measure the longitudinal energy distribution curve. Experimental results are presented and compared to simulated results by utilising a custom designed tracking code.

Keywords: Photocathodes, Energy spread, Electron sources, Electrostatics

I. ENERGY DISTRIBUTION OF PHOTOEMITTED ELECTRONS

It has long been known that the quality of a beam delivered to a free electron laser (FEL) is limited by the electron source and the optics transporting this beam[1]. Photoemission is the technique of choice for high-performance pulsed electron sources, and despite being a well-established technique for generating electron beams, studies into photocathode materials are still an active area of research[2].

An electron emitted from a photocathode will have some excess energy after overcoming the workfunction of the material with velocity components in both the longitudinal and transverse planes with respect to the surface normal. Figure 1 shows how the longitudinal and transverse velocities are defined in relation to an electron emitted from a photocathode. In the non-relativistic regime the velocity v and electron mass m_e are related to the kinetic energy ε through the standard formula:

$$\varepsilon = \frac{1}{2} m_e v^2 \tag{1}$$

With reference to figure 1 and equation 1, we define transverse energy ($\varepsilon_\perp$) as the energy associated with velocity in the x-y planes (parallel to the photoemitter surface) and the longitudinal energy ($\varepsilon_\parallel$) as that associated with the velocity component in the y-z plane (perpendicular to the photoemitter surface). It follows that the total energy of a photoemitted electron is the sum of the transverse and longitudinal energy, i.e:

$$\varepsilon = \frac{1}{2} m_e v^2 = \frac{1}{2} m_e (v_\perp^2 + v_\parallel^2) = \varepsilon_\perp + \varepsilon_\parallel \tag{2}$$

As a result of the many complicated processes that take place during photoemission such as scattering in the migration to the surface (electron-electron scattering in the case of metal photocathodes and electron-phonon scattering for semiconductor photocathodes), and other factors at the cathode-vacuum interface (such as diffraction and surface roughness), photoemitted electrons will have a distribution of energies. As such, longitudinal and transverse energy distribution curves (LEDC and TEDC, respectively) can be measured to characterise photoelectrons. An ideal electron source is one that produces a cold beam, i.e., small mean energy spreads. Whilst a reduction in transverse energy spread is desirable in electron beams driving FELs, it is clearly important to understand photoemission in both transverse and longitudinal planes to understand the photoemission process as a whole. Given that the total energy spread in a photoemitted electron beam is conserved with its upper limit defined primarily by the illumination photon wavelength, the photocathode band gap and the workfunction of the surface, knowledge of the LEDC is complementary to that of the TEDC. Furthermore, as this work

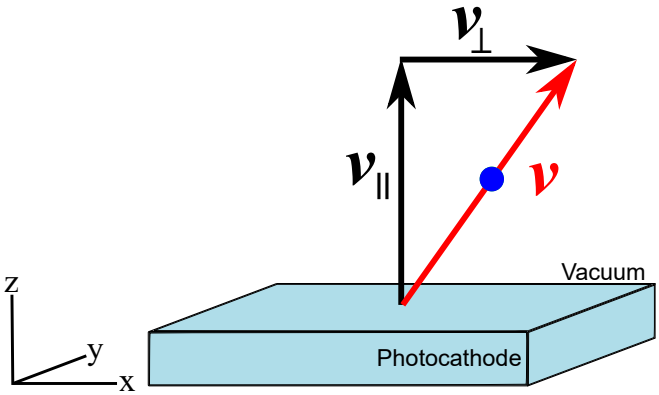

FIG. 1. An electron emitted from a photocathode into the vacuum will have velocity components $v_\perp$ in the transverse (x-y) and $v_\parallel$ in the longitudinal (z) planes, derived from their transverse and longitudinal energy components.

shows, the measurement of an LEDC is substantially easier than that of a TEDC provided that a directly-measurable photocurrent can be extracted from the photocathode.

Several systems have been established world-wide to measure the energy spread of various photocathode materials[3–6]. The Transverse Energy Spread Spectrometer (TESS) experiment, built by ASTeC, is one such system. During commissioning of the instrument, TESS was used to measure the TEDC from gallium arsenide[7]. TESS has also been used to study the evolution of LEDC and TEDC of gallium arsenide phosphide photocathodes as a function of their degradation state[8].

In this work we present the comparison of a simulation modelling the measurement of an LEDC in TESS with actual experimental data, and assess the instrument's suitability to perform this task. In section II the TESS experimental setup is described and in section III we discuss computational methods to model the experiment. Section IV describes how TESS may be used to measure the longitudinal energy distribution of photoemitted electrons and presents experimental results using the system, and in section V electron transport is studied through simulations.

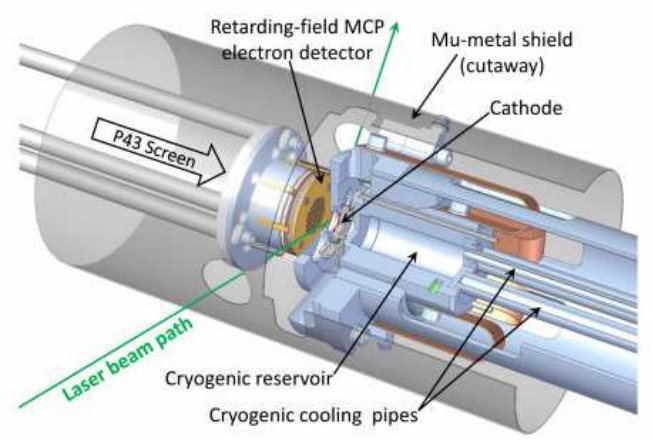

FIG. 2. Cut-away showing the TESS photocathode source and detector system[7]. At the centre, a cathode is placed in a holder ans emits electrons when illuminated by laser light. Wire meshes are used to generate a static electric field between the source and detector which extracts electrons from the cathode and accelerates them towards the detector system. A mu-metal casing shields the experimental region from external magnetic fields, and the facility for cryogenic cooling allows measurements to be performed at liquid nitrogen temperatures. Reproduced from Proceedings of FEL2013[7].

II. TRANSVERSE ENERGY SPREAD SPECTROMETER (TESS)

TESS combines a source electrode with a photocathode holder which permits the exchange of photocathodes under test. The photocathode can be illuminated by a laser or a broadband light source. The photoemitted electrons are accelerated away from the cathode towards a detector assembly by an electrostatic field generated by applying a potential to a set of wire meshes. The detector contains a microchannel plate (MCP) coupled to a phosphor screen. A signal is recorded either directly for an LEDC as a measurement of photocurrent from the MCP front or optically for a TEDC as the photoemission footprint from the phosphor screen using a CCD camera. A cut away of the TESS structure is shown in figure 2 and an exploded view of the detector is shown in figure 3, with a schematic overview of the complete system shown in figure 4.

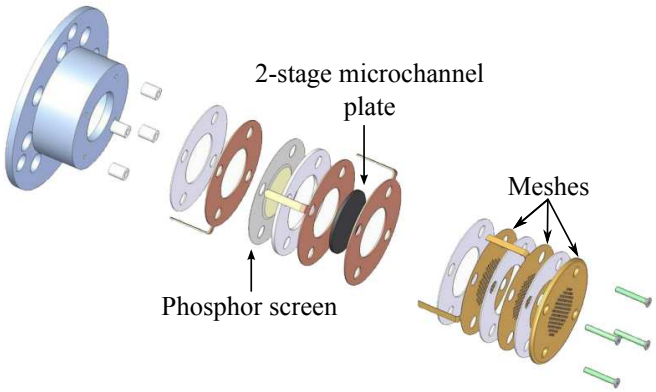

FIG. 3. Exploded view of the wire meshes and MCP/fluorescent phosphor screen detector system. Reproduced from Proceedings of FEL2013[7].

A. Photocathode Electron Source

The source electrode holds an interchangeable 10 mm ⌀ photocathode puck at its centre, and can be biased at up to -1 kV DC to create a uniform electric field in the vicinity of the cathode. A laser system installed externally to the TESS vacuum chamber illuminates the photocathode at a grazing angle of $\sim 17^\circ$ with respect to the cathode surface plane. The laser beam passes through an opening in a mu-metal magnetic shield which is mounted on the cathode electrode, and is thereby held at the source potential during operation. The laser system comprises interchangeable solid-state laser modules which can provide illumination at a number of wavelengths (532, 635, 670, 780 and 808 nm), with optics to deliver a focused beam of typically 120-140 μm FWHM. The laser spot size can be verified using a beam profile camera located on the optical board whose CCD array is placed at the equivalent working distance as the cathode surface inside the TESS chamber. Laser light intensity is controlled through the use of neutral density filters so only a small photocurrent is extracted from the cathode to avoid the effects of space charge on the dynamics of the emitted electron beam. Additional TESS capabilities include cryogenic cooling of the cathode holder so that photocathodes can be tested at liquid nitrogen temperature (-196 °C), and the inclusion of a piezo-electric leak valve which allows controlled degradation through gas exposure of the photocathode under test.

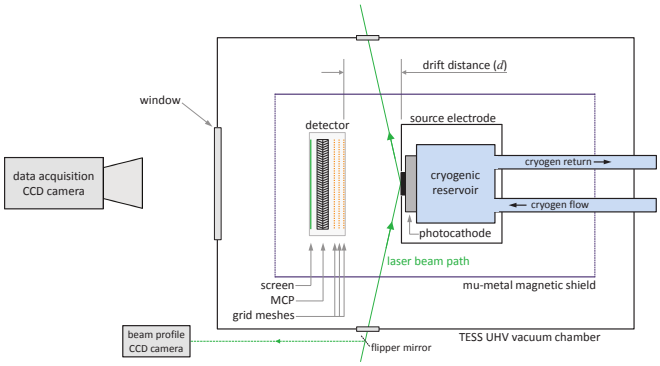

FIG. 4. Complete schematic of TESS. The system consists of: a cathode plug and holder with a cryogenic system to cool the photocathode to liquid nitrogen temperature; a detector system which includes three wire meshes (from right to left m1, m2 and m3), a two-stage MCP and a phosphor screen; an externally mounted laser system which is directed into TESS through a small window; and a CCD camera system which is used when a signal is detected optically. The inner chamber of TESS is enclosed in a mu-metal shield and housed inside a UHV vacuum chamber.

B. Electrostatic Mesh Grids

The front of the detector assembly comprises three mesh grids, with the detector front plate and the first mesh being electrically common. The meshes were photo-etched from a tungsten sheet 35 μm thick and comprise mesh cells with pitch 500 μm, wire thickness of 50 μm and a trimming radius between orthogonal wires of 50 μm, as shown in figure 5. The meshes are coated with gold which has a lower secondary electron yield compared to tungsten, and ensures good electrical conductivity whilst being non-magnetic. The distances between the first (m_1) and second (m_2) meshes and the second and third (m_3) meshes are 1.3 mm and 1.4 mm, respectively. The meshes are electrically isolated, and can be biased at levels up to $\pm$1 kV.

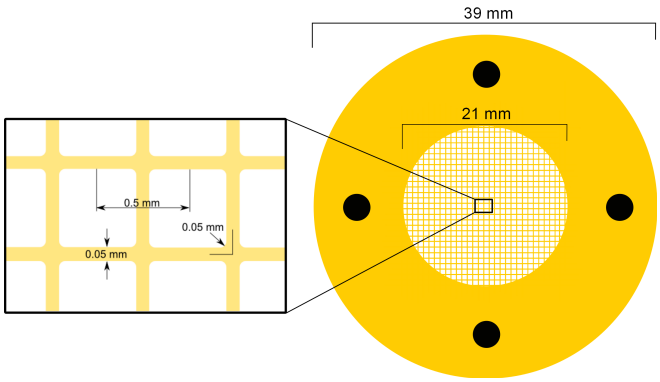

FIG. 5. Gold-coated tungsten wire mesh photoetched from a 35 μm sheet. The mesh cell has a pitch of 500 μm with a bending radius of 50 μm at the corners with a wire thickness of 50 μm. The meshes are held in place by by four non-magnetic rods.

C. Electron Detector

The imaging system of the detector assembly contains a two-stage micro-channel plate (MCP) (Hamamatsu F1094-01) and a P43 ITO phosphor screen. The MCP amplifies the electron signal with a gain in the range of $10^4/10^7$ depending on the applied front-back potential which can be up to 2 kV. The phosphor screen can be operated at up to 6 kV, and converts the electron output from the MCP into a fluorescent image showing the photoemission footprint with a quoted spatial resolution of between 80 and 100 μm. The drift space distance between the cathode source and the detector assembly is adjustable between approximately 7.5 and 50 mm, and the combination of this drift space distance and the specific voltages applied to the source and the first mesh grid determines the size of the photoemission footprint on the entrance of the detector and consequently on the phosphor screen.

D. Data Acquisition

Data is acquired optically for a TEDC measurement from the phosphor screen using a 14 bit CCD camera (PCO.2000)[9] located outside of the vacuum chamber., The LEDC measurement does not use the phosphor screen and camera, and simply uses the MCP front plate to make a direct measurement of the photoemitted current.

In the TEDC optical method, the photoemission footprint is imaged onto the camera CCD array using a Tamron f3.5 180 mm lens[10] and a Nikon x2 teleconverter. The CCD array is cooled and operates at around -20 °C, with the camera boasting a high dynamic range and extremely low noise signature. The camera is mounted on a vibration-free frame allowing long exposure times. The CCD quantum efficiency is $\sim$ 50 % at the 543 nm peak emission wavelength of the phosphor screen.

In the direct LEDC method, the photoemitted current is measured from the MCP front plate, effectively using it as a charge collector. The photocurrent is measured using a lock-in amplifier (SR830 by Stanford Research Systems)[11] whereby the SR830 modulates the laser light at a frequency of 1 kHz and uses phase sensitive detection to effectively filter out the background contribution and provide femto-Ampere precision in the photocurrent measurement.

Both the source and detector assemblies fit inside the mu-metal shield cylinder (see figure 2), though its shielding from external magnetic fields is not perfect as both ends of the cylinder are open. Further openings have been machined into the shield to allow photocathode insertion/extraction, and the entry of laser light to drive electron emission.

Gallium arsenide photocathodes designed for use in the 4GLS[12] and the ALICE particle accelerator upgrade[13,14] were used for the measurements and results presented in this article, but other cathode materials, particularly multi-alkali and metals are envisaged to be tested in the near future. The Photocathode Preparation Facility (PPF)[15,16] located next to TESS facilitates the production of high quantum efficiency GaAs

photocathodes which are then transferred under XHV conditions directly into the TESS chamber.

III. ELECTROSTATIC WIRE MESH SIMULATION CODE

To fully understand the transport of photoelectrons within the TESS structure, including the fields generated by wire meshes, a combination of field calculations using the finite element method solver Comsol Multiphysics[17] with a customised particle tracking code written in Matlab Simulink[18] were used. A more complete description of the tracking code is given elsewhere[19].

A good understanding of the fields generated around the wire meshes is critical as they strongly affect the motion of electrons within the experiment. An analytical equation of the potential surrounding a wire mesh has been established[20] but requires assumptions to be made which limit the applicability to physical systems. For this reason finite element solvers are used to computationally calculate potentials and forces around a wire mesh, in this case using the exact geometry of the TESS meshes. To be confident of the solutions calculated with Comsol, crosschecks were performed with Opera[21], another electromagnetic simulation package, which gave good agreement.

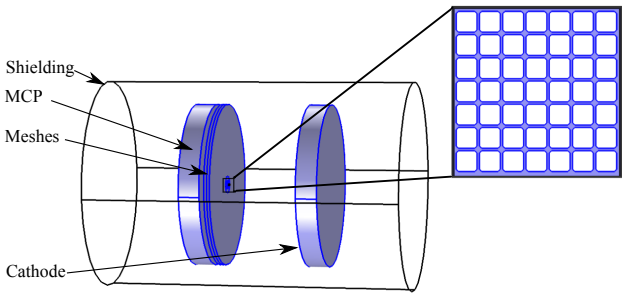

FIG. 6. Schematic of the TESS 3D model built in Comsol Multiphysics. The model includes three meshes, a cathode, a microchannel plate and the mu-metal outer shielding. The mesh, MCP and cathode plates are modelled as cylinders and the meshes are modelled as thin cylinders with cells cut out. The inset depicts a 7 x 7 structure used to represent a full mesh structure. The geometry of the mesh cells are the same as those shown in figure 5 and the distance between the meshes and the MCP are the same as those given by the manufacturer.

Through a finite element convergence study it was found that approximately 5.5 million elements were required to fill one channel through three meshes to obtain a converged solution. As a result it was not possible to solve a full mesh assembly on a desktop computer due to computer memory limitations. To overcome this, the solution around one cell channel can be calculated and repeated for all channels within the model. A convergence study was performed in which increasing number of cells were included in the model until the solutions converge to obtain a close approximation to a full wire mesh system. It was found that a 7 x 7 array was sufficient to represent a full mesh system. A three dimensional model of TESS, built in Comsol, is shown in figure 6. The cathode is modelled as a single object at one potential, rather than the cathode and holder in the actual TESS chamber, and the MCP is modelled as a flat surface rather than with an array of micron sized channels running through the structure. The inset in figure 6 shows a 7 x 7 array of wire mesh cells.

A tracking code was developed for this study which allows any initial particle velocity distribution to be simulated using fields generated either analytically or using a finite element solver. The code numerically solves the equation of motion using the Runge-Kutta method to track particles from the cathode through TESS to predict the trajectory of any photoemitted electron (i.e. detected, retarded or stopped on part of a wire mesh), or it may be used to monitor particular properties during a simulation, e.g. transverse velocity. If an electron arrives at a wire or the front of the MCP it remains there for the remainder of the simulation and is effectively 'lost'. As a consequence of the extremely low current drawn from the photocathode which is typically in the order of 10 fA (approximately 10^5 electrons per second, each with a source-detector flight time of < 25 ns), particle–to–particle Coulomb repulsion ('space charge') does not need to be considered despite the highly-focussed lightsource driving photoemission.

IV. METHODOLOGY AND EXPERIMENTAL RESULTS

Initial plans to measure the LEDC involved using the wire meshes as an energy filter (a Retarding-Field Analyser). However, experimental and simulated results shown in a previous article[22] indicated that the signal reduced over an energy range far too large to be wholly attributed to the LEDC alone. This has since been attributed to the fields produced around the wire meshes which prevent the use of this technique to measure the LEDC. A new technique was then proposed which involves sweeping the photocathode bias voltage from an initial level where photoemission is inhibited (close to 0.0 V where the cathode is effectively reverse biased) to a final negative level where the cathode is emitting its maximum photocurrent. All three of the meshes and the MCP front plate are held at constant positive potentials during the measurement, with the aim of extracting and efficiently transporting photoemitted electrons from the source to the MCP. The photocurrent is measured from the MCP front plate as a function of the source potential, and the first derivative of this curve shows the longitudinal energy distribution of the photoelectrons.

Experiments were performed using TESS with fixed mesh potentials (m_1, m_2 and m_3) for three different configurations. The MCP front potential was kept at 0.0 V while the cathode potential was swept and the total photoemitted current was then measured from the MCP front plate. The electron source under test was a GaAs photocathode with initial quantum efficiency around 4 % at 635 nm wavelength. Our photocathode preparation facility had been vented and baked shortly prior to this experiment, so the environment was not optimal for the preparation of semiconductor photocathodes.

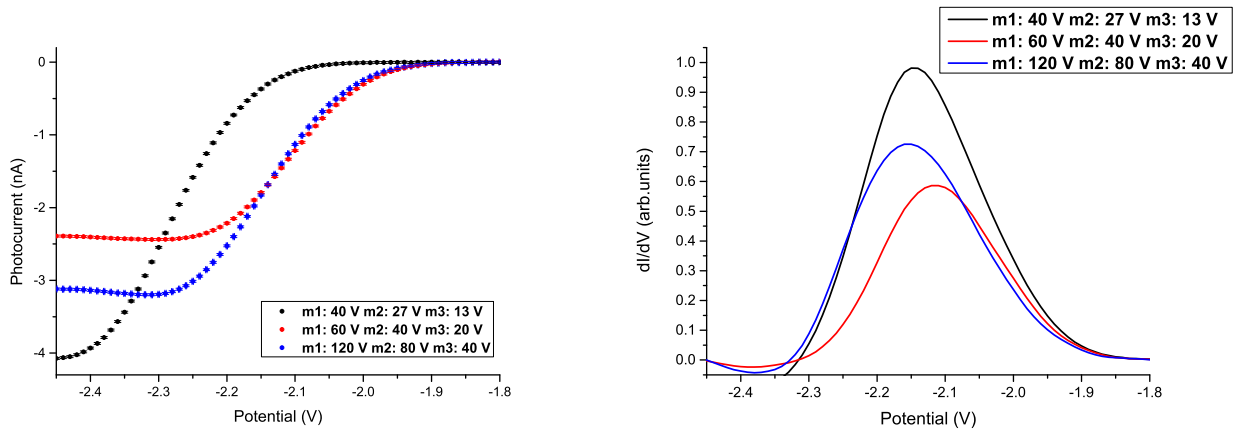

(a) (b)

FIG. 7. a) I-V curve of the measured photocurrent from modulation of the cathode potential with three different mesh potential configurations as indicated in the legend with no forced degradation of the photocathode. b) Normalised LEDC for three mesh potential configurations found by differentiating the I-V curves.

Figure 7a shows the current-voltage (I-V) curves obtained for three different mesh potential configurations applied to provide effective electron transport from source to detector. Measurements were taken in the following order: black curve, blue curve and red curve. The reduction in photocurrent signal most likely occurs due to degradation of the quantum efficiency due to short photocathode lifetime rather than the difference in mesh configurations. It is possible to extract the longitudinal energy spread by differentiating the I-V curve. This is shown in figure 7b where the experimental data set has been smoothed using a moving average filter. The curves obtained are near Gaussian and fitting such to each curve yields their standard deviations, and therefore values for the longitudinal energy spread which were 83.4 meV, 83.4 meV and 87.7 meV for the black, red and blue line configurations, respectively. This suggests that the choice of mesh potentials have little or no effect on the final energy spread measurement. This should be expected since the energy spread is an intrinsic property of the photoemitted electrons, and neither the potential difference between the cathode or the MCP, or the path taken between them affect this, i.e. the potential merely controls transport from the source to the MCP front plate. These results are consistent with other experiments on GaAs using a single wire mesh[23]. It should be noted that the negative values of the potentials in figures 7a and 7b are due to the contact potential difference between the various materials of the system. This is constant during the short duration of an experiment. The shape of the curve, however, is more important since it holds information of the kinematics of the photoemitted electrons.

V. SIMULATION RESULTS AND COMPARISON WITH EXPERIMENT

To further understand the transport from the cathode to the detector system we used the code described in section III. The experimental I-V curves show that the cathode went from full emission to fully reversed-biased within 0.6 V. To simulate this technique a series of electric field maps were generated by changing the cathode plate voltage in steps of -0.01 V from 0.0 V to -0.6 V. An initial longitudinal energy distribution was then generated for 100,000 particles using a Gaussian distribution with parameters found experimentally (figure 7b). This produces a distribution of longitudinal energies up to approximately 600 meV. We assume all electrons are emitted with approximately the same total energy, equal to the most energetic electrons in the longitudinal plane, with a deviation of 5 % to account for small variations. The transverse energy for each electron was then assigned by using equation 2.

Figure 8 shows a colourmap of the values of the initial longitudinal and transverse energies which were assigned to electrons in this simulation. The combined initial distribution (colourmap) differs to that previously reported[24], however, assigning energy spread in this way provides a simple method to test the technique in extracting the information about longitudinal energy of photoemitted electrons. To be sure that this technique works correctly we would expect that characteristics of the longitudinal energy distribution can be extracted from MCP front plate current measurements as a function of source voltage.

Photoemission was simulated by initially releasing only the most energetic electrons from the cathode into the model space, and progressively releasing more electrons on each voltage step. This process was repeated until -0.6 V is applied to the photocathode plate where all electrons were simulated in-flight. A normalised comparison of simulated and experimental LEDC curves is shown in figure 9. Since we do not

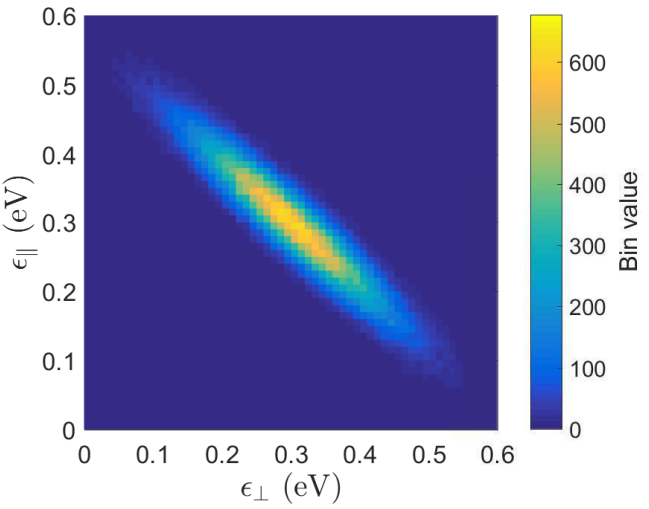

FIG. 8. Colourmap showing the corresponding longitudinal and transverse energies that were simulated.

account for the contact potential difference in the model, two x-axes are used for both the simulated and experimental cases. The simulated curve returns a Gaussian profile with standard deviation of 84.0 meV. As the initial simulated LEDC has a standard deviation of 83.4 meV (black curve) we can therefore see that the LEDC profile is maintained from the cathode to the charge collector. Differences between the experimental and simulated curves in the figure are due to the experimental data being approximated to a Gaussian when deriving input energy profiles for the simulations.

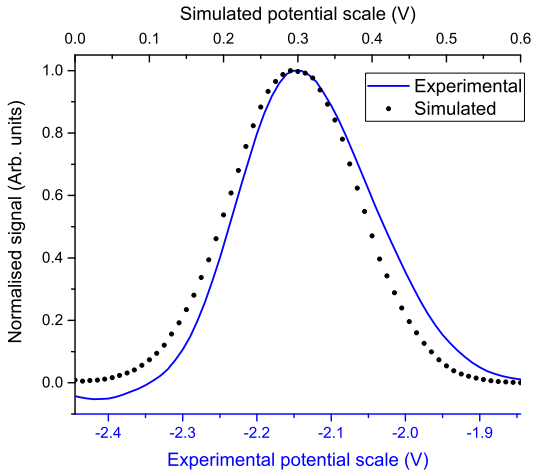

FIG. 9. Comparison of a simulated LEDC (black points) with that obtained from experiment (blue curve). Simulations do not take into account the contact potential difference, hence the use of the dual x-axes.

Since we are unable to known where the laser exactly impinges on the cathode we wished to know if this impacted the results. We therefore simulated two cases the first with the emission centroid aligned with the centre of the wire meshes,

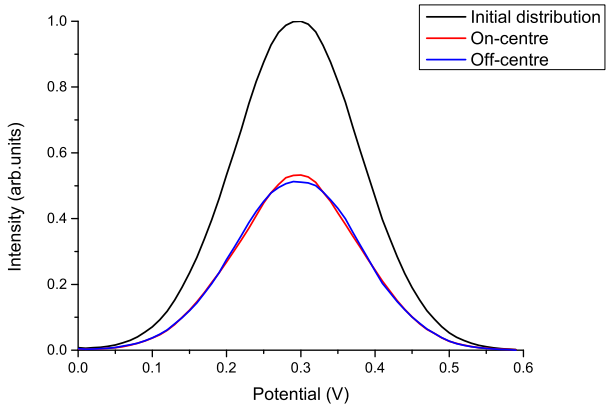

FIG. 10. LEDC curves for different initial emission points compared to the initial LEDC put into the simulation.

and the second with the emission point off-centre with respect to the mesh grid. The curves normalised to the initial distribution obtained are shown in figure 10. As a result of mesh collisions a reduced number of electrons reach the MCP front plate with the off-centre case recording the lowest signal. Fitting a Gaussian to the two simulated curves yields standard deviations of 84.0 mV and 85.0 mV for the on-centre and off-centre case, respectively. The standard deviation of the initial distribution sampled was 84.6 mV and both simulated results agree within 95 % confidence bounds. This indicates that while transport efficiency from the cathode to the MCP front plate is slightly reduced, the overall result is not affected by the alignment of the emission point with respect to the mesh grid. It can be seen in figure 10 that the detected signal is approximately half of the initial distribution. The manufacturer quotes a transmission through a mesh to be 80 % so for three meshes the transmission should be 51.2 % therefore signal reduction by a factor of 2 is to be expected.

VI. SUMMARY AND CONCLUSIONS

In this paper we have investigated the longitudinal energy distribution of photoemitted electrons in low energy beams through direct measurement using the TESS experimental system and compared the results with the predictions of a 3D model.

The initial plan was to use the multi-mesh system of TESS as a field-retarding analyser. This method was later deemed impractical and a new technique was devised using the same system. The new method creates a potential difference between the cathode and meshes to accelerate and transport photoemitted electrons to the MCP front plate. The cathode bias was progressively adjusted from an initial level which forced a state of zero emission to a final level which permitted full electron emission. Through simulations it has been shown that the energy distribution profile is maintained during transport from the cathode to the charge collector. This technique

is therefore the primary method used to measure the LEDC of electrons in the TESS experimental system.

Planned modifications to the TESS system include reducing the number of installed meshes for longitudinal energy spread measurements from three to just one since the retarding-field analyser technique has been has been ruled out. This is expected to increase the detector performance for both LEDC and TEDC measurements as the transmission through the 3-mesh system is around 51 % while the transmission through a single mesh is around 80 %.

ACKNOWLEDGMENTS

We would like to thank Dr Heinrich Scheibler (Institute of Semiconductor Physics, SB RAS, Novosibirsk, Russia) for his assistance during measurement taking and proposing the measurement technique. This work was supported by the STFC Cockcroft Core Grant No. ST/G008248/1.

[1] G. Penco, E. Allaria, L. Badano, P. Cinquegrana, P. Craievich, M. Danailov, A. Demidovich, R. Ivanov, A. Lutman, L. Rumiz, P. Sigalotti, C. Spezzani, M. Trov, and M. Veronese, "Optimization of a high brightness photoinjector for a seeded FEL facility," *Journal of Instrumentation*, vol. 8, no. 05, p. P05015, 2013.

[2] D. H. Dowell, I. Bazarov, B. Dunham, K. Harkay, C. Hernandez-Garcia, R. Legg, H. Padmore, T. Rao, J. Smedley, and W. Wan, "Cathode R&D for future light sources," *Nuclear Instruments and Methods in Physics Research A*, vol. 622, pp. 685–697, Oct. 2010.

[3] S. Zwickler, D. Habs, P. Krause, S. Pastuszka, D. Schwalm, A. Wolf, and A. S. Terekhov, "Energy analysis of electrons emitted by a semiconductor photocathode," in *In *Stanford 1993, Proceedings, Photocathodes for polarized electron sources for accelerators* 446-455*, 1994.

[4] U. Weigel, *Cold intense electron beams from gallium arsenide photocathodes*. PhD thesis, University of Heidelberg, 2003.

[5] T. Vecchione, I. Ben-Zvi, D. H. Dowell, J. Feng, T. Rao, J. Smedley, W. Wan, and H. A. Padmore, "A low emittance and high efficiency visible light photocathode for high brightness accelerator-based x-ray light sources," *Applied Physics Letters*, vol. 99, no. 3, 2011.

[6] S. Karkare, L. Cultrera, Y.-W. Hwang, R. Merluzzi, and I. Bazarov, "2-D energy analyzer for low energy electrons," *Review of Scientific Instruments*, vol. 86, no. 3, 2015.

[7] L. Jones, R. Cash, B. Fell, , J. McKenzie, K. Middleman, B. Militsyn, H. Scheibler, D. Gorshkov, and A. Terekhov, "The commisioning of TESS: An experimental facility for measuring the electron energy distribution from photocathodes," in *Proceedings of FEL2013*, 2013.

[8] L. B. Jones, H. E. Scheibler, D. V. Gorshkov, A. S. Terekhov, B. L. Militsyn, and T. C. Q. Noakes, "Evolution of the transverse and longitudinal energy distributions of electrons emitted from a gaasp photocathode as a function of its degradation state," *Journal of Applied Physics*, vol. 121, no. 22, p. 225703, 2017.

[9] PCO. http://www.pco.de.

[10] Tamron. http://www.tamron.co.uk.

[11] Stanford Research Systems. http://www.thinksrs.com/.

[12] J. Clarke, "The conceptual design of 4GLS at Daresbury Laboratory," in *Proceedings of EPAC 2006*, pp. 181–183, 2006.

[13] M. Poole and E. Seddon, "4GLS and the prototype energy recovery linac project at Daresbury 4GLS.," in *Proceedings of 2005 Particle Accelerator Conference*, pp. 455–457, 2005.

[14] B. Militsyn, I. Burrows, R. Cash, B. Fell, L. Jones, J. McKenzie, K. Middleman, S. Kosolobov, H. Scheibler, and A. Terekhov, "Design of an upgrade to the ALICE photocathode electron gun," in *Proceedings of 2008 European Particle Accelerator Conference*, pp. 235–237, 2008.

[15] B. Militsyn, I. Burrows, R. Cash, B. Fell, L. Jones, J. McKenzie, K. Middleman, H. Scheibler, and A. Terekhov, "High voltage DC photoinjector development at Daresbury Laboratory," *ICFA Beam Dynamics Newsletter*, 2010.

[16] B. Militsyn, I. Burrows, R. Cash, B. Fell, L. Jones, J. McKenzie, K. Middleman, H. Scheibler, and A. Terekhov, "First results from the iii-v photocathode preparation facility for the alice erl photoinjector," in *Proceedings of IPAC'10*, (Kyoto, Japan), 2010.

[17] Comsol Multiphysics. www.comsol.com/.

[18] Mathworks. http://mathworks.com/.

[19] L. J. Devlin, O. Karamyshev, and C. P. Welsch, "Charged particle tracking through electrostatic wire meshes using the finite element method," *Physics of Plasmas*, vol. 23, no. 6, 2016.

[20] L. J. Devlin, *Studies towards an enhanced understanding of electron beams and their diagnostics*. PhD thesis, The University of Liverpool, 2016.

[21] Opera. www.operafea.com/.

[22] L. J. Devlin, O. Karamyshev, C. P. Welsch, L. B. Jones, B. L. Militsyn, and T. C. Q. Noakes, "Measurements of the longitudinal energy distribution of low energy electrons," in *Proceedings of IPAC 2014*, pp. 720–723, 2014.

[23] L. B. Jones, S. A. Rozhkov, V. V. Bakin, S. N. Kosolobov, B. L. Militsyn, H. E. Scheibler, S. L. Smith, and A. S. Terekhov, "Cooled Transmission-Mode NEA-Photocathode with a Band-Graded Active Layer for High Brightness Electron Source," in *American Institute of Physics Conference Series*, vol. 1149 of *American Institute of Physics Conference Series*, pp. 1057–1061, 2009.

[24] D. Orlov, M. Hoppe, D. Schwalm, A. Terekhov, and A. Wolf, "Longitudinal and transverse energy distributions of electrons emitted from GaAs(Cs,O)," *Applied Physics Letters*, vol. 78, no. 18, pp. 2721–2723, 2001.